Design and analysis of a compact EUV interferometric lithography system

Bruce W. Smith
Rochester Institute of Technology
Microsystems Engineering
82 Lomb Memorial Drive
Rochester, New York 14623
E-mail: bwsemc@rit.edu

Abstract. A small-scale interferometric EUV exposure system is presented, based on Talbot interferometric imaging. In this approach, illuminated EUV grating mask orders are recombined remotely through reflection, resulting in interference with spatial preservation across the image plane. The approach is achromatic for NA=λ/p using parallel recombination mirrors and is superior to other methods when efficiency and alignment tolerances are considered. The system design is compatible with both a compact EUV plasma source, which can yield exposure times on the order of several minutes per field, and a compact resonant cavity EUV laser source, which can produce exposure times on the order of several seconds. The system is capable of resolution to 15 to 30-nm half-pitch and is adjustable to accommodate targeted values in this range. Field size is approximately 1 mm, which is consistent with the current field size offered on 193-nm immersion interferometric systems. Wafer stage technology allows for nanometer positioning control across the field and through a field depth of over 50 μm. EUV mask grating fabrication requirements are within the current state of the technology, where no grating component requires resolution better than 2× the image plane pitch (a full-frequency doubled system). Reflection technology has been utilized for each component of the interferometer unit. While the grating mask employs $(SiMo)^{40}$ multilayers, the interferometric turning mirrors are metallic coatings at angles sufficient to achieve reflection efficiencies greater than 80% for 15-nm half-pitch resolution. The efficiency of the interferometric head is between 7 and 29%, much higher than that which can be achieved using other interferometric lithography (IL) methods. Vibration control for the EUV-IL15 is achieved through a state-of-the-art piezoelectric active isolation system to achieve vibration criteria levels at 1/3 vibration control level E. © 2009 Society of Photo-Optical Instrumentation Engineers. [DOI: 10.1117/1.3134094]

Subject terms: EUV; interferometric lithography (IL); nanolithography; sub-32 nm; Talbot.

Paper 08155SSRR received Oct. 6, 2008; revised manuscript received Mar. 27, 2009; accepted for publication Apr. 1, 2009; published online Jun. 2, 2009.

1 Introduction

As nanolithography progresses into sub-32-nm device generations, EUV technology is generally identified as the most likely imaging method. As the insertion point is pushed to ever-decreasing dimensions, the technical challenges increase. Some of the key challenges are the fundamental ones, including photoresist materials and patterning processes. Resists must exhibit the required image resolution with high throughput and low line edge roughness (LER). This is very difficult, as these dimensions are approaching the physical limits of modulation and diffusion for conventional chemically amplified resist (CAR) photoresists. There is a clear need for small-scale exposure tools that can deliver the resolution required for resist and patterning research and development (R&D), similar to what has been successfully carried out at optical deep ultraviolet (DUV) wavelengths (190 to 250 nm). The most recent small-scale nanolithography R&D systems have been built based on interferometric imaging.[1,2] Through the use of two- and four-beam interferometric lithography (IL) technology combined with a variety of optical material types and immersion fluids, resolution down to 26-nm half-pitch at 1.86 NA has been achieved.[3] Extending these IL concepts to the EUV is a natural progression.[4] The challenge of EUV IL for resist and patterning R&D is to provide a system that is compact and affordable for photoresist and materials research groups.

1932-5150/2009/$25.00 © 2009 SPIE

2 Interferometric Lithography (IL) for EUV Patterning

In interferometric imaging, a sinusoidal intensity standing wave pattern is created when two coherent wavefronts interfere. The pitch or period (p) of the grating is determined by

$$\text{Pitch} = \lambda/(2 \sin \theta), \quad (1)$$

where θ is the incident half-angle of the wavefronts. Through control of the interference angle, pitch values can be varied to values as small as $\lambda/2$. Since no collection or

Downloaded from SPIE Digital Library on 27 Jan 2010 to 129.21.240.32. Terms of Use: http://spiedl.org/terms

projection optics are utilized, accompanying optical aberrations are eliminated. The depth of field (DOF) is determined by the source beam coherence, diameter, intensity profile, and angle of intersection. Matched amplitude values result in ideal contrast with unity modulation. This can be reduced through control of the imaging depth beyond the DOF.

The requirements of an IL system can follow several configurations. For example, a Lloyd's mirror approach has been demonstrated with the highly coherent EUV radiation from a beam line.[4] This wavefront-splitting method consists of flat mirror(s), from which is reflected a portion of the wavefront coming from a source. Another portion of the wavefront proceeds directly from the source to the recording plane. For a separation distance between the source and the second effective sources (a), interference is created where the pitch of the grating image is $s\lambda/a$. Alternatively, an amplitude-splitting imaging interferometer system would basically consist of a beamsplitter and two reflecting mirrors. When a source beam is incident on the beamsplitter, part of the beam is transmitted and part is reflected. After splitting, the two wavefronts travel along separate identical paths. Interference of the waves results in a periodic intensity distribution, which is imaged as a grating structure in a photoresist layer. To reduce the presence of extraneous interference fringes, a source with a very narrow spectral bandwidth is needed. This is difficult for EUV, as is the careful alignment control, intensity matching, and polarization matching that must be achieved. These are formidable challenges for EUV sources, which can exhibit low spatial and temporal coherence. Amplitude-splitting interferometry can be made practical for EUV application, however, through careful achromatic design considerations that preserve as much spatial coherence as possible.

2.1 *Consideration of EUV-IL Approaches*

A primary challenge for a compact IL system for EUV wavelengths is the poor spatial and temporal coherence properties of currently available compact plasma sources. Achromatic approaches similar to those used at longer DUV wavelengths have been proposed to circumvent such problems. Alternatively, a compact coherent laser source can be pursued that offers appropriate levels of spatial and temporal coherence. The challenge is then to choose the best IL design for resolution, throughput, and robust performance.

There are several approaches to achromatic interferometric lithography. Two specific achromatic designs are potential candidates for EUV-IL:

- A holographic mask approach using dual mask gratings, where the second grating combines $\pm$ first orders from the first grating. The suitability of these approaches for EUV-IL is carried out through the evaluation of across-field and through-field imaging as well as radiometric throughput.
- A Talbot interferometric approach in which ± 1 grating mask orders are recombined remotely to the mask through reflection, resulting in interference with the spatial preservation across the image plane. This approach is achromatic for $\mathrm{NA}=\lambda/p$ using parallel recombination mirrors.

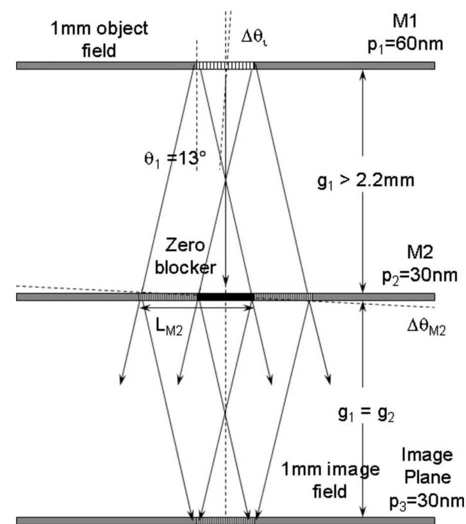

Fig. 1 A schematic of an achromatic EUV holographic mask approach to interferometric lithography.

2.1.1 *The holographic mask approach*

Several designs have been developed using a phase mask to diffract radiation mainly into two first orders for recombination at an image plane. In many instances, a phase shifting effect is accomplished using a binary grating mask with provisions to remove the resulting zero-order, undiffracted beam. Although this method results in a throughput loss on the order of 50%, it is often the most practical or only solution available. By employing such a zero-order blocker, the configuration of a system requires additional complexity, adding for example a second mask grating for recombination. For use in the EUV, the constraints of mask and system geometry limit the feasibility of this holographic method to a double grating approach.

First introduced by Anderson et al.[5] and later improved by Yen et al.,[6] the dual-mask achromatic holographic configuration has been shown to be capable of very high resolution imaging at excimer laser wavelengths. Such a holographic approach makes use of the amplitude and phase distribution of a coherent wave distribution. The availability of matched fused silica binary and phase shift masks, together with the alignment tolerances allowed at excimer laser wavelengths, has also led to the development of variations on this theme for immersion lithography, as described by Charley et al.[7]

A critical analysis has been carried out for the dual-mask achromatic holographic configuration for application at 13.5 nm. The basic dual-mask system configuration is shown in Fig. 1, where an EUV source is used to illuminate a 1-mm field on a transmission grating mask. The pitch on the first mask $M1$ is $2\times$ at 60 nm (30-nm hp), whereas the pitch on the second mask is $1\times$ at 30 nm (15-nm hp) to produce a desired pitch of 30 nm at the image plane. The diffracted first-order angle is 13 deg, which requires a first-to-second mask gap g_1 and the second mask to image plane gap g_2 of 2.2 mm or greater for the 1-mm field. The total gap error $\Delta(g_1+g_2)$ for a 3-deg subtended angle $(\Delta\theta_i)$ is

Downloaded from SPIE Digital Library on 27 Jan 2010 to 129.21.240.32. Terms of Use: http://spiedl.org/terms

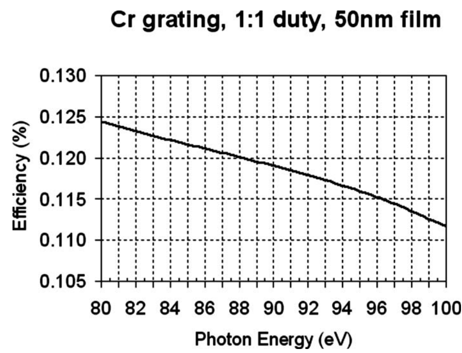

Fig. 2 The calculated efficiency for a 1:1 chromium grating mask at EUV wavelengths. The efficiency at 13.5 nm is 12%.

$$\Delta(g_1 + g_2) = \frac{(p^2 - \lambda^2)^{1/2}}{\Delta\theta_i} = 515 \text{ nm}, \quad (2)$$

which represents the entire error budget in gauging and depth of field (DOF). The $M2$ grating length L_{M2} is $4g_1(\tan\theta_1)$, or greater than 2 mm. If the Δg_1 error budget is 50% of the total, the maximum allowable rotational gauging error for mask $M2$ is very small at

$$\Delta\theta_{M2}(\max) = \tan^{-1}\frac{\Delta g_1}{L_{M2}} = 0.128 \text{ mrad} = 0.007 \text{ deg}, \quad (3)$$

and the DOF at the image plane (Δg_2) is low at 257 nm. When $g_1 = 5$ mm, the maximum rotational error is 0.003 deg (0.052 mrad). One of the challenges with the dual-mask achromatic holographic configuration lies with the strict specifications on gauging and alignment. Although these levels may be within the state of the art for ultra-precision motion and staging control, they are at the limits and one to two orders of magnitude greater that those that would be desirable in order to build, align, and operate a robust system.

Additionally, the design of a EUV dual-mask approach requires the use of transmission masks, which can present several problems over reflective counterparts. The efficiency of a 1:1 chromium grating mask is shown in Fig. 2, where a mask of 50-nm film thickness exhibits about 12% throughput at 92 eV (13.5 nm). Furthermore, the transmission of 100-nm Si membrane is 84%, yielding a 10% total grating efficiency. The thermal loading on such a mask requires additional study, as it can be prone to distortion, especially as it is employed at the second mask plane $M2$. Also, as with any transmission window placed in the path of high spatial coherence (as will be achieved through selection of this small subtended angle), diffractive artifacts will result. With no practical means for spatial filtering in the EUV beam path, it is expected that these artifacts will lead to degradation of image quality in the image plane.

Possibly the largest mask-related challenge with this IL approach is with the resolution requirements for the second grating mask. Since this system is not a reduction system, a transmissive EUV mask with 15-nm half-pitch defined patterns must be fabricated. This represents a significant challenge. Additional fabrication challenges are also introduced

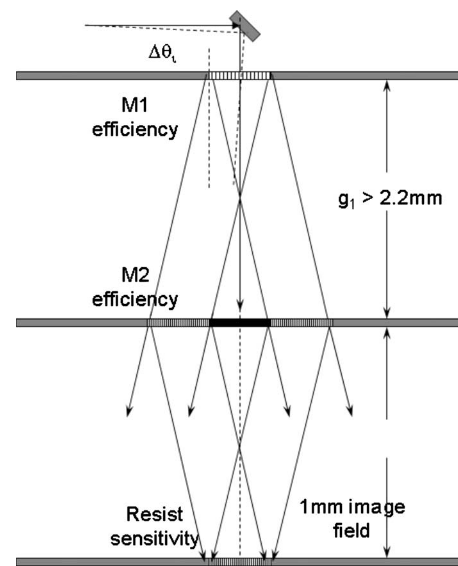

Fig. 3 Radiometric considerations for the achromatic EUV holographic mask approach.

with higher order gratings. It is not anticipated that this system could be extensible to sub-15-nm half-pitch resolution.

Radiometric analysis has also been carried out for the dual-mask configuration, as shown in Fig. 3. Throughput is broken down by components including the collection efficiency, turning mirror efficiency, collector loss ($R^n = 0.64^4$), mask $M1$ and $M2$ throughput (0.1^2), and resist sensitivity (20 mJ/cm^2). For a ± 10 deg illuminated angle from the source, a four-mirror collector is assumed to achieve a subtended angle between 2 and 4 deg, a 1-mm mask and image field, a 20-mJ/cm^2 sensitive resist, and with no other alignment or gauging errors, throughput can be calculated. Based on an ideal setup, the resulting power density is 2 to 20 mW/cm^2, and the required exposure time is 1 to 10 s per field.

More realistic calculations can be made by considering the practical requirements of a robust system. The depth of field (DOF) for 30-nm pitch interference at the image plane is a function of the field location and the relative rotational error of the second grating mask ($\Delta\theta_{M2}$). For a total DOF ($g_1 + g_2$) of 515 nm (for a 3-deg subtended source angle case using collection optics and a 10-deg illuminated angle), the DOF falls to zero at 0.13 mrad error, or 0.007 deg. This can be seen in Fig. 4. For a 0.3-deg subtended source angle, the DOF increases proportionally to a more reasonable value of 5 μm. As the subtended source angle decreases by 10×, exposure time increases by 100×. Compared to 3 deg for a 5-s exposure, 0.3 deg corresponds to a 500-s or 8.3-min. exposure. There is clearly a trade-off between system complexity and performance, and the anticipated throughput benefit of the dual-mask holographic method over other methods could be quickly lost as alignment requirements and restrictions are considered. In general, the expected system performance can be summarized in Table 1.

Downloaded from SPIE Digital Library on 27 Jan 2010 to 129.21.240.32. Terms of Use: http://spiedl.org/terms

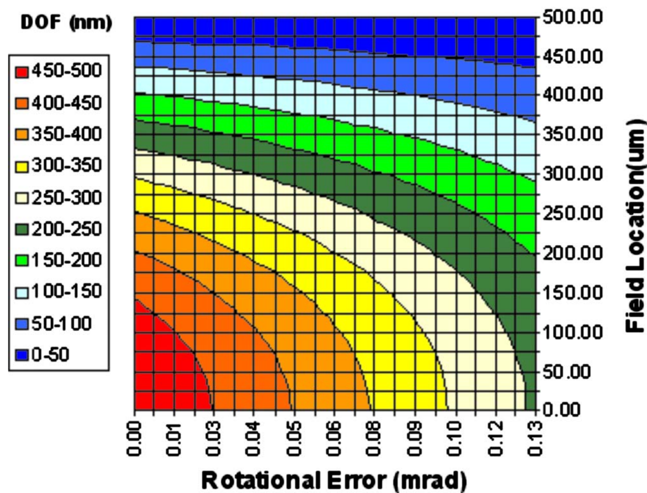

Fig. 4 Depth of field (DOF) for the achromatic EUV holographic mask approach plotted for field locations from 0 to 0.5 mm with *M*1 rotational error to 0.128 mrad (0.007 deg). This is for a best-case geometry where $g_1 = g_2 = 2.2$ mm.

2.1.2 *The Talbot EUV-IL approach*

The demanding alignment and mask resolution tolerances of the single- and dual-mask holographic techniques can be substantially reduced by incorporating a grating mask into a Talbot interferometer. This approach has also been developed and demonstrated for various applications.[8–10] Most recently, the Talbot method has been employed in a Smith-Talbot interferometer design for excimer laser wavelengths.[11,12]

Through Talbot interference, a symmetric achromatic configuration can be designed to best satisfy the mutual coherence requirements of a weakly coherent source. The interferometer design employs a grating mask (either a phase grating or a binary grating with a zero-order blocker) and turning mirrors to recombine diffraction orders, most commonly the +1st and −1st. With a mirror angle chosen for equal conjugates (unity magnification or $\mathrm{NA} = \lambda / p$), the orders split by diffraction and are recombined with spatial preservation.

The configuration is shown in Fig. 5. The system is fully frequency doubling, where the mask requirements for 30-nm pitch imaging are 2×, or 60 nm. This is an important advantage of this approach and represents current levels of the state of the art, where extensibility to smaller geometry is also possible. The achromatic behavior can be shown though the calculation of the image pitch (p_2) achieved from a mask pitch (p_1), together with the mirror tilt error ($\Delta\theta_M$) as

$$p_2 = \left\{ \frac{2\cos(2\Delta\theta_M)}{p_1} + 2\sin(2\Delta\theta_M)\left[\frac{1}{\lambda^2} - \frac{1}{p_1^2}\right]^{1/2} \right\}^{-1}. \tag{4}$$

When the tilt error is zero, the pitch is independent of wavelength and the system is achromatic:

Table 1 The predicted performance for a dual-mask holographic IL approach. Values are calculated for an ideal configuration, unless otherwise noted. The depth of field (DOF) is defined as 50% of the entire gap error budget, where 50% is attributed to the *M*2 alignment error budget. The error in alignment between *M*1 and the image plane is included in the DOF.

General properties of a dual-mask IL system for 30-nm pitch imaging	
*M*1 mask pitch	60 nm
*M*2 mask pitch	30 nm
Min. gapping (g_1, g_2)	2.2 mm
Track length	4.4 mm
Total gap error for 3 deg illum. angle (DOF+Δg_1)	515 nm
Min. *M*2 grating length	2 mm
Max. *M*2 rotation error (50% budget)	0.007 deg
DOF for 2-mm gapping (50% budget)	257 nm
Max. *M*2 rotation error (for 5-mm gapping)	0.003 deg
Power density for 10 deg collection (3 deg subtended)	1 to 20 mW/cm2
Exposure time for 3 deg subtended	2 to 10 s
DOF for 0.3 deg subtended (2-mm gap, 50% budget)	5 μm
Power density 0.3 deg subtended	0.02 to 0.2 mW/cm2
Exposure time for 0.3 deg subtended	3 to 17 min

$$p_2 = \frac{p_1}{2}. \tag{5}$$

As tilt errors are considered, the source bandwidth needs to be accounted for, leading to some practical limitations to the achromatic behavior. For a spectral bandwidth $\Delta\lambda = \lambda_a - \lambda_b$, and corresponding p_a and p_b, the beat period P_B will determine the usable image field size, where

$$P_B = \left(\frac{1}{p_a} - \frac{1}{p_b}\right)^{-1}. \tag{6}$$

When $\Delta\lambda$ is small compared to p_1 (and assumed to be 0.27 nm compared to 60 nm, or 0.45%), the beat period, P_B, becomes

$$P_B = l_c[2\sin(2\Delta\theta_M)\cos(\theta_i)]^{-1}. \tag{7}$$

Furthermore, the fringe contrast across the field becomes

Downloaded from SPIE Digital Library on 27 Jan 2010 to 129.21.240.32. Terms of Use: http://spiedl.org/terms

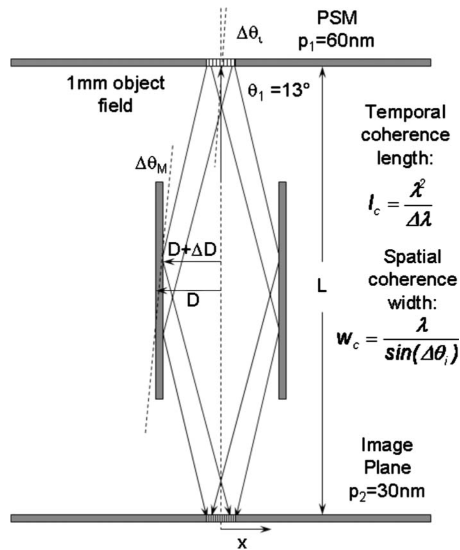

Fig. 5 A schematic of the imaging conditions of a Talbot EUV-IL approach using ±1 grating mask orders are recombined remotely to the mask through reflection, resulting in interference with the spatial preservation across the image plane. The approach is achromatic for NA=λ/p using parallel recombination mirrors.

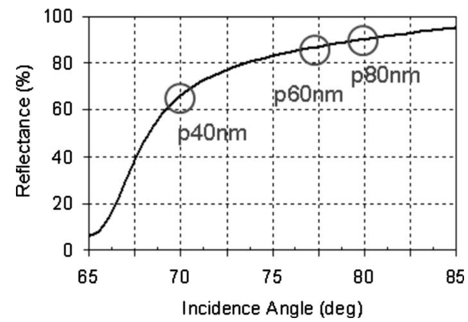

Fig. 6 The reflectance of a metallic molybdenum mirror at 13.5 nm at angles of incidence corresponding to diffraction angles for various mask pitch values.

$$C = \left| \cos \frac{\pi x}{P_B} \right|. \tag{8}$$

The depth of field (DOF) on center can be determined from the spatial coherence width (w_c), which is related to the subtended source angle ($\Delta\theta_i$), the wavelength, and p_2 by

$$\text{DOF} = \frac{p_2 w_c}{\lambda} = \frac{p_2}{\sin(\Delta\theta_i)}. \tag{9}$$

Analysis of an achromatic Talbot EUV-IL system is carried out based on several system assumptions. A fundamental requirement of the system is the ability to print 15-nm half-pitch geometry. Both a compact EUV plasma source and a highly coherent resonant cavity EUV laser were considered in the analysis. The use of a compact 10 to 15 W electrodeless z-pinch EUV plasma source[13] provides a low throughput or interim solution using a commercially available source. A resonant cavity EUV laser system could provide the coherence and power necessary for higher throughput via shorter exposure times. Coherent source requirements would include high in-band power greater than 100 μW with a repetition rate on the order of 200 MHz. Such a system could be the natural extension of a concept that has been successfully demonstrated at longer EUV wavelengths, where 100-MHz output from 60 to 120 nm has already been achieved.[14] The use of intracavity high harmonic generation in the EUV would provide sufficient output for application to interferometric imaging. Additional assumptions used in the analysis of the EUV-IL system include the following:

1. The achromatic Talbot design is used for achromatic operation and preservation of spatial coherence across the field.
2. A bandwidth of 2% is used for all cases (plasma and laser).
3. ± first grating orders are used for frequency doubling (60-nm period to 30-nm pitch); the zero order is blocked for the binary grating mask.
4. The turning mirror and reflective mask efficiency are based on $(\text{Si/Mo})^{40}$ multilayers.
5. The reflective phase grating is based on a $(\text{Si/Mo})^{40}-(\text{Si/Mo})^{54}$ stack π phase shift.
6. Interferometer mirrors are based on a Mo thin film, 85% R for 77-deg angle from a 60-nm-period grating mask (see Fig. 6).
7. Error in the interferometer mirror angle ($\Delta\theta_M$) reduces the field size. (A 0.01-deg error is assumed achievable.)
8. Designs are for a 1-mm field with a 90% contrast subfield greater than 200 μm.
9. The plasma source is treated as a point source irradiating into a hemisphere.
10. The resonant cavity laser power is into a 1-mm beam and spatial coherence is more than 8 mm.
11. A depth of field (DOF) greater than 20 μm with 90% contrast is desirable.
12. A resist sensitivity of 20 mJ/cm^2 is assumed.
13. Field exposure times less than 3 min are desirable.

The radiometric throughput of the system can be calculated using Fig. 7 and the throughput of the various components. This includes the efficiencies of the turning mirror, the pinhole, the mask, and the interferometer arms, as well as the resist sensitivity. No collector optics are used, as no benefit would be provided, which simplifies the system substantially. Several circumstances are evaluated by considering the use of a binary transmission mask, a binary reflection mask, and a phase shift reflection mask together with compact plasma and resonant cavity laser EUV sources. This analysis follows, where the exposure time, field size, depth of field, and number of full cycles for 90% contrast are calculated. Additionally, plots of the fringe contrast versus field size and depth of field are presented. The image performance across and through the field is a function of the source coherence and therefore changes only as the plasma and laser sources are compared.

Downloaded from SPIE Digital Library on 27 Jan 2010 to 129.21.240.32. Terms of Use: http://spiedl.org/terms

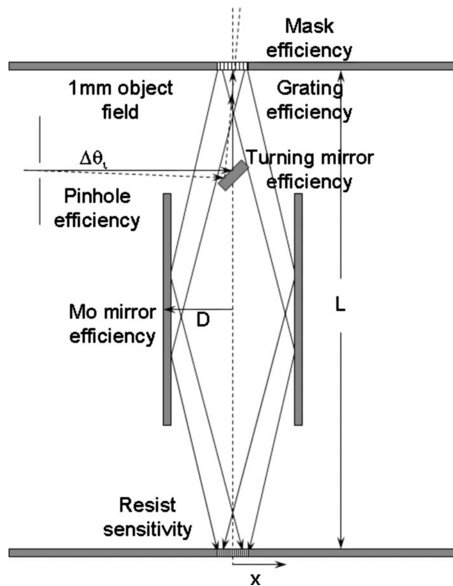

Fig. 7 A schematic for radiometric considerations of a Talbot EUV-IL approach.

Figure 8 shows the field performance for the Talbot EUV IL for use with a 10-W compact plasma source. As can be seen, the full field size is 992 μm. The subfield size for 60% contrast is reduced within this field to 600 μm, and the subfield size for 90% contrast is 300 μm, both within reason for a small-field R&D system. The depth of field is 57 μm, which is reduced to 35 μm for 60% contrast and 16 μm for 90% contrast. Although these values present challenges over what could be achieved with higher coherence, they are reasonable and well within the range attainable with nanopositioning stages. It should be noted that the DOF for the Talbot method is 100 to 1000× greater than what can be achieved using a dual-mask holographic approach.

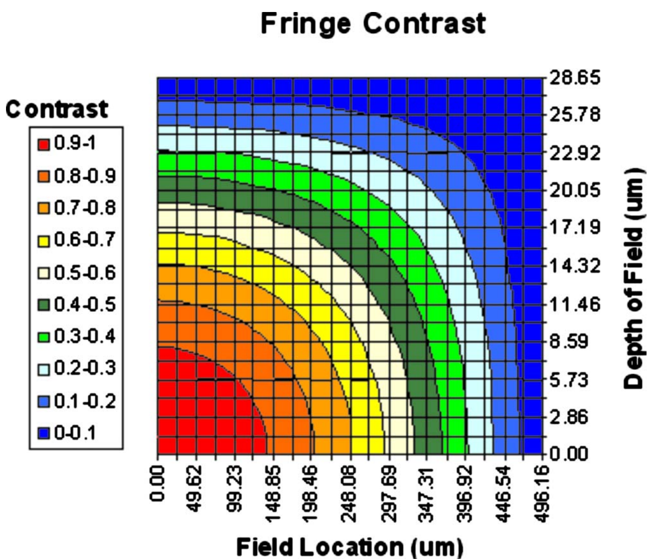

Fig. 8 The field performance for the EUV IL with a compact EUV plasma source.

Table 2 Summary of the throughput performance of the EUV-IL12 with various source and mask configurations.

Configuration	Exposure time
Plasma source—reflective binary mask	32 min
Plasma source—reflective phase mask	8 min
Plasma source—transmissive mask	136 min
Laser source—reflective binary mask	22 s
Laser source—reflective phase mask	5 s
Laser source—transmissive mask	1.5 min

The field performance for the EUV-IL can be improved through the use of a 100-μW resonant cavity EUV laser source. The full field size remains at 992 μm, which is a function of the source bandwidth and is conservatively defined at 2%, matching that for the plasma source. Subfield dimensions also do not change. The depth of field is substantially larger, however, reducing restrictions on the image plane and making the system much more robust and stable. The DOF is 300× greater than for the plasma source, or 17 mm.

Radiometric calculations for EUV-IL approaches using a reflective binary mask and a phase shift mask with a plasma source and a resonant cavity laser source have been carried out to determine exposure time requirements, which are summarized in Table 2.

3 EUV-IL System Design

The EUV IL is shown schematically in Fig. 9. The system is fully enclosed in an environmental chamber with amine contamination filtering integrated into the systems filter fan unit for protection against airborne molecular acids, bases, and condensable organic compounds. The exposure unit is

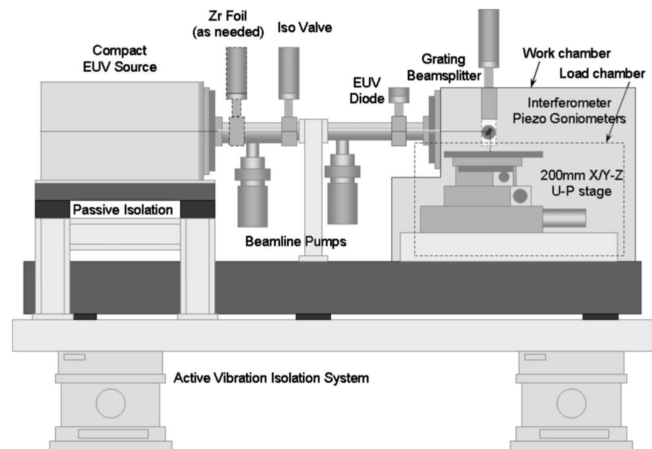

Fig. 9 A schematic of the EUV-IL15 compact interferometric lithography tool.

Downloaded from SPIE Digital Library on 27 Jan 2010 to 129.21.240.32. Terms of Use: http://spiedl.org/terms

isolated from vibration using an active vibration isolation system and a design to ensure minimal vibration transmission in critical components. The system is designed for use with a compact resonant cavity laser source but can be fitted with a compact plasma source for low-volume, low-throughput use. When a plasma source is used, Zr foil debris mitigation is incorporated into the beamline. Additionally, a the 2π subended angle from the source is reduced through a pinhole, mounted near the plasma source, and optimized in order to reduce spatial coherence artifacts within the beam.

The interferometer is designed around the achromatic Talbot approach. The head design is compact to ensure minimum path length error between the two arms but sufficiently large to allow for gauging and alignment. The turning mirrors incorporate nanofabricated alignment grating targets to enable rotational accuracy within the level required by the system. The system uses two EUV power meters, one at the beamline entrance into the work chamber and a second near the reflective mask plane.

The ultra-precision positioning stages are designed to control x,y, and z motion with submicrometer precision. Stage travel in the x and y directions is 105 mm, allowing for an active area on the wafer substrate greater than 75 mm. Accuracy is 250 nm over 50 mm of travel, sufficient for die placement and SEM inspection/metrology of processed wafers in the full image field of the system. Precise z-axis (height) control is carried out through closed loop nanopositioning stages with accuracies to 100 nm or through piezoelectric control to 50 nm. The travel range of the z-axis stages is 26 mm, which is within the requirements for stage height location for user-controlled image pitch selection.

Image pitch (resolution) is controlled through the translation of the mask stage and the selection of grating subfields. The EUV reflective mask is comprised of up to four subfields, each approximately 50 mm^2, with grating periods between 60 nm and 120 nm for image plane resolution between 15-nm and 30-nm half-pitch, respectively. (Other values are also possible, based on the design and fabrication of the mask.) The mask subfields are adjacently located on the mask, allowing selection by linear displacement of the mask holder in steps of approximately 7 mm. Micrometer positional accuracy is sufficient, which is accomplished using a small bidirectional linear reticle stage. As the mask pitch is selected, the corresponding diffracted field requires the adjustment of the wafer plane z-axis stage. For example, as the selected half-pitch resolution is changed from 15 nm to 30 nm, a z-axis stage height adjustment on the order of 20 mm is carried out. The method of pitch selection with the system allows for automated reconfiguration for maximum flexibility. Furthermore, through the control of the z-axis stage height, image demodulation can be controlled within the system to carry out defocus. Through the adjustment of the z-axis wafer and mask stage height, image demodulation can be controlled within the system to carry out defocus experiments or run focus-exposure series for resist and image process evaluation. Correlation between the depth of field of the system for the selected pitch and the depth of focus for an EUV projection lithography system is required. Additional flexibility is possible with the system, as it is configured with the coherent EUV resonant cavity laser. The latitude made possible with the laser source allows for single-beam attenuation within the interferometer for programmed two-order interference exposure combined with the demodulation of single-arm, single-beam exposure. The correlation between 2+1 beam demodulation to defocus is carried out within the operation software through lookup tables, created using lithographic simulation software to synthesize various conditions of imaging.

4 Conclusions

This analysis of achromatic EUV interferometric systems affords limited opportunities but a clear path toward a system that can provide appropriate resolution, contrast, field size, throughput, flexibility, and robust performance for research and development applications. A Talbot EUV-IL design offers the greatest performance and flexibility and has been chosen as the preferred direction for a compact lithography system for 15-nm half-pitch resolution. A compact plasma source approach can provide a low-throughput solution using a reflective phase mask, where:

1. The field exposure time is 8 min, which could be reduced to 5 min with a 15-W source. Exposure times are 50% lower, or 2.5 min, if a 10 mJ/cm^2 resist is assumed.
2. The full field size is approximately 1 mm with a $\sim$300 μm subfield size for greater than 90% image contrast.
3. The depth of field is $\sim$17 μm at the center of the field (for 90% contrast) and $\sim$14 μm at 50 μm from the center of the field.
4. The low spatial coherence of the plasma source will result in an increase in sensitivity to misalignment error in interferometer arms.
5. The resulting field will print approximately 5000 full pitch cycles with contrast better than 90% at best focus.
6. A mirror alignment error of 0.1 deg (versus 0.01 deg) reduces full field size to $\sim$0.1 mm (10%) and 90% contrast field size to $\sim$30 μm. This is not anticipated, as the 0.01 deg control is within the state of the art.

A resonant cavity laser source can provide a higher throughput solution with a reflective or transmissive mask, where:

1. A reflective phase mask leads to highest throughput with 5-s field exposures (or 2.5 s for a 10 mJ/cm^2 resist).
2. The field size (all cases) remains sufficiently large at $\sim$1 mm with $\sim$300-μm subfield size with greater than 90% contrast.
3. The depth of field is 17 mm, which is substantial. Finding focus and alignment at the image plane will not be an issue, alignment error of interferometer arms is not as critical.
4. Mirror alignment tolerance is unchanged.

Downloaded from SPIE Digital Library on 27 Jan 2010 to 129.21.240.32. Terms of Use: http://spiedl.org/terms

References

1. J. A. Hoffnagle, W. D. Hinsberg, M. Sanchez, and F. A. Houle, "Liquid immersion deep-ultraviolet interferometric lithography," *J. Vac. Sci. Technol. B* **17**(6), 3306–3309 (1999).
2. B. W. Smith, A. Bourov, Y. Fan, F. Cropanese, and P. Hammond, "Amphibian XIS: an immersion lithography microstepper platform," in *Optical Microlithography XVIII*, B. W. Smith, Ed., *Proc. SPIE* **5754**, 751–759 (2005).
3. B. W. Smith, Y. Fan, M. Slocum, and L. Zavyalova, "25-nm immersion lithography at a 193-nm wavelength," in *Optical Microlithography XVIII*, B. W. Smith, Ed., *Proc. SPIE* **5754**, 141–147 (2005).
4. H. H. Solak, D. He, W. Li, S. Singh-Gasson, F. Cerrina, B. H. Sohn, X. M. Yang, and P. Nealey, "Exposure of 38 nm period grating patterns with extreme ultraviolet interferometric lithography," *Appl. Phys. Lett.* **75**, 2328–2330 (1999).
5. E. H. Anderson, K. Komatsu, and H. I. Smith, "Achromatic holographic lithography in the deep ultraviolet," *J. Vac. Sci. Technol. B* **6**(1), 216–218 (1988).
6. A. Yen, E. H. Anderson, R. A. Ghanbari, M. L. Schattenburg, and H. I. Smith, "Achromatic holographic configuration for 100-nm-period lithography," *Appl. Opt.* **31**(22), 4540–4545 (1992).
7. A. L. Charley, A. Lagrange, O. Lartigue, J. Simon, P. Thony, and P. Schiavone, "Hyper high numerical aperature achromatic interferometer for immersion lithography at 193 nm," *J. Vac. Sci. Technol. B* **23**(6), 2668–2674 (2005).
8. Talbot, *Philos. Mag.* **9**, 401 (1836).
9. Rayleigh, *London, Edinburgh Dublin Philos. Mag. J. Sci.* **11**, 196 (1881).
10. P. E. Dyer, R. J. Farley, and R. Giedl, "Analysis of a 0/1 order Talbot interferometer for 193 nm laser grating formation," *Opt. Commun.* **129**, 98–108 (1996).
11. B. W. Smith, "Reduction Smith-Talbot interferometer prism for micropatterning," U.S. Patent No. 7,170,588 (2007).
12. A. Bourov, Y. Fan, F. Cropanese, N. Lafferty, L. Zavyalova, H. Kang, and B. W. Smith, "Immersion microlithography at 193 nm with a Talbot prism interferometer," *Proc. SPIE* **5377**, 1573–1578 (2004).
13. S. F. Horne, M. M. Besen, D. K. Smith, P. A. Blackborow, and R. D'Agostino, "Application of a high-brightness electrodeless Z-pinch EUV source for metrology, inspection, and resist development," *Proc. SPIE* **6151**, 61510P (2006).
14. C. Gohle, T. Udem, M. Herrmann, J. Rauschenberger, R. Holzwarth, H. A. Schuessler, F. Krausz, and T. W. Hansch, "A frequency comb in the extreme ultraviolet," *Nature (London)* **436**, 234–237 (2005).

Bruce W. Smith is the Intel Professor and Director of Microsystems Engineering at the Rochester Institute of Technology (RIT) where he has been involved with teaching and research in microlithography, thin films, optics, materials, and nanopatterning for more than 20 years. He received his PhD degree from RIT and has worked with various groups and organizations including Sematech and IMEC. He has published over 100 technical papers and several textbook chapters and holds over 20 patents. He is a fellow of SPIE and a member of OSA, IEEE, and AVS.

Downloaded from SPIE Digital Library on 27 Jan 2010 to 129.21.240.32. Terms of Use: http://spiedl.org/terms